Journal of Applied Geophysics 111 (2014) 256–270

Contents lists available at ScienceDirect

Journal of Applied Geophysics

journal homepage: www.elsevier.com/locate/jappgeo

Two-dimensional nonlinear geophysical data filtering using the multidimensional EEMD method

Chih-Sung Chen, Yih Jeng *

Department of Earth Sciences, National Taiwan Normal University, 88, Sec. 4, Ting-Chou Road, Taipei, 116, Taiwan, ROC

ARTICLE INFO

Article history:
Received 17 January 2014
Accepted 13 October 2014
Available online 27 October 2014

Keywords:
Geophysical data processing
Nonlinear filtering
2DEMD
Multidimensional
EEMD
Multivariate EMD

ABSTRACT

A variety of two-dimensional (2D) empirical mode decomposition (EMD) methods have been proposed in the last decade. Furthermore, the multidimensional EMD algorithm and its parallel class, multivariate EMD (MEMD), are available in recent years. From those achievements, it is possible to design an efficient 2D nonlinear filter for geophysical data processing. We introduce a robust 2D nonlinear filter which can be applied to enhance the signal of 2D geophysical data or to highlight the feature component on an image. We did this by replacing the conventionally used smooth interpolation in the ensemble empirical mode decomposition (EEMD) algorithm with a piecewise interpolation method. The one-dimensional (1D) EEMD procedures were consecutively performed in all directions, and then the comparable minimal scale combination technique was applied to the decomposed components. The theoretical derivation, model simulation, and real data applications are demonstrated in this paper. The proposed filtering method is effective in improving the image resolution by suppressing the random noise added in the simulation example and strong low frequency track corrugation noise bands with background noise in the field example. Furthermore, the algorithm can be easily extended to higher dimensions by repeating the same procedure in the succeeding dimension. To evaluate the proposed method, one data set is processed separately by using the enhanced analytic signal method and the multivariate EMD (MEMD) algorithm, and the results from these two methods are compared with that of the proposed method. A general equation for generating three-dimensional (3D) EEMD components based on the comparable minimal scale combination principle is derived for further applications.

1. Introduction

Conventional filtering methods mostly are applications of the Fourier analysis or a newer approach, wavelet analysis (Foufoula-Georgiou and Kumar, 1994; Jeng et al., 2011; Stollnitz et al., 1995). In recent years, the empirical mode decomposition (EMD) technique is rapidly developing as a new tool in data analysis and filtering. The EMD is an adaptive, data-driven nonlinear data processing method which decomposes data into mono-component signal. Since it was invented by Huang et al. (1998), this method has evolved from the prototype to a variety of EMD based data processing algorithms in exploration geophysics and engineering (Battista et al., 2007; Jeng and Chen, 2011, 2012; Jeng et al., 2007; Lin and Jeng, 2010; Macelloni et al., 2011, Rehman and Mandic, 2010a,b,c; Xue et al., 2013; Zhou et al., 2012). However, most of the published algorithms are one dimensional or pseudo-two-dimensional (pseudo-2D). In general, the pseudo-2D EMD method manages 2D data as a set of one dimensional traces, and analyzes each trace using conventional one dimensional (1D) EMD algorithm. After decomposing each trace of the data, the components of the same sifting level in each trace are sorted out to one gather to construct a pseudo-2D EMD component (Han and van der Baan, 2013; Huang, 2001) or pseudo-2D EEMD (ensemble empirical mode decomposition) component (Chen and Jeng, 2011, 2013; Jeng and Chen, 2011). As proposed by Wu and Huang (2009), the EEMD technique is a noise assisted data analysis method to alleviate the mode mixing problem caused by the intermittent signal. The pseudo-2D approach is successfully used in analyzing temporal–spatial (one temporal dimension and one spatial dimension) data or two dimensional spatial data polarized in one direction and without intermittency. For the data lacking distinguishable directionality or being intermittent, the functionality of the pseudo-2D EMD analysis is drastically limited, and the analyzed results will be unstable and exhibiting obvious inter-slice discontinuity (Wu et al., 2009). Although the intermittent problem can be overcome by employing the pseudo-2D EEMD technique (Wu and Huang, 2009; Wu et al., 2009), the inter-slice discontinuity still remains.

Various real 2D EMD algorithms have been proposed during the last decade. They include using radial basis functions as basis vectors for constructing 2D surface (Nunes et al., 2003, 2005), making use of Delaunay triangulation and piecewise cubic interpolation for 2D decomposition (Damerval et al., 2005), applying the variable sampling

* Corresponding author. Tel.: +886 2 77346416; fax: +886 2 29333315.
E-mail address: geofv001@ntnu.edu.tw (Y. Jeng).

http://dx.doi.org/10.1016/j.jappgeo.2014.10.015
0926-9851/

and thin plate spline techniques to two dimensional interpolation (Linderhed, 2005), employing the finite element method in two dimensional surface fitting (Xu et al., 2006), and so on. Although the stated approaches differ greatly, the essential idea is to fit surfaces rather than to fit curves when sifting the data. In other words, a surface envelope will replace the line envelope in the 2D EMD data sifting. These new methods have made significant progresses in the 2D EMD analysis, but some basic problems persist. The major difficulties of determining the surface envelope by using the aforementioned new two-dimensional algorithms are the uncertainty of determining the optimum local extrema, the huge cost of computation, and the problem of mode mixing (Bhuiyan et al., 2009; Wu et al., 2009). To determine the optimum local extrema and take control of the mode mixing problem, Wu et al. (2009) presented their multidimensional EEMD (MDEEMD) algorithm which applies the one-dimensional EEMD analysis sequentially to the data in each dimension to obtain a collection of multidimensional components, and then combines the appropriate components based on the minimal scale combination strategy to attain a set of MDEEMD filter bank. This method skillfully circumvents the difficulties of finding the optimum local extrema in multidimensional data, and eliminates the mode mixing. In particular, it is easy to apply. Even though the MDEEMD method performs better than many other methods, some difficulties need further study, mainly the spline technique. The cubic spline used in the MDEEMD is efficient but may introduce false extrema during the sifting process, and the end effect from the spline envelope can cause unexpected errors.

In parallel to the development of multidimensional EMD, the multivariate EMD (MEMD) for time series analysis is also emerging (Neukirch and Garcia, 2014; Rehman and Mandic, 2010c, 2011; Rehman et al., 2013). The MEMD originates from the idea of bivariate EMD for processing complex signals (Rilling et al., 2007; Tanaka and Mandic, 2007). It follows the development of trivariate EMD (Rehman and Mandic, 2010a), quadrivariate EMD (Rehman and Mandic, 2010b), and MEMD related algorithms. These methods can also help to solve the aforementioned unstable and inter-slice discontinuity problems of the pseudo-2D EMD to a large extent.

In fact, the multidimensional EMD and the MEMD are strongly correlated. The concept of oscillations in EMD is generalized to be rotations (Mandic et al., 2013), and the sifting and envelope interpolation procedures are similar in both methods. The basic difference is the way of determining the local maxima and minima because the MEMD tries to alleviate the problem of numbers that are not ordered. In other words, the MEMD helps solve issues involving numbers that are undefined or cannot be compared with one another (e.g. complex numbers). The MEMD algorithm transfers the data into real-valued signals by employing a signal projecting technique, and generates multivariate envelope curves by using the rotation invariant EMD (RIEMD) algorithm which defines the extrema based on a change in the phase rather than the amplitude of the signal (Looney and Mandic, 2009). By calculating the mean of the multivariate envelope curves, the multivariate signal mean is obtained for EMD sifting. Because the approach considers extrema in several directions, it generates an equal number of IMFs for each channel of the data that makes it easier for processing multidimensional data. Similar in spirit to EEMD, an updated version of the MEMD (the ensemble MEMD) has been proposed in the context of time series analysis but has not been applied directly to the multidimensional data (Rehman et al., 2013). More detailed discussions of the multidimensional EMD and the MEMD can be found in Mandic et al. (2013).

Given that the images can be vectorized, the vectorized EMD schemes like MEMD or bivariate EMD can be applied.

The focus of this paper is to apply the MDEEMD technique with modifications to make it more feasible in the 2D geophysical data processing, especially in the application of data filtering. As it has been pointed out by the inventors of the EMD and the related methods, the EEMD usually bring in nonzero noise elements which are impossible to remove completely (Wu and Huang, 2009). Based on our experiences, the remaining noise could be exaggerated through improper use of the spline technique. This imperfection may introduce unreliable intrinsic mode functions (IMFs) (Appendix A) and end effect problems. To avoid drawbacks of the spline technique used in most of the EMD related algorithms, the piecewise cubic Hermite interpolating polynomial (PCHIP) spline is adopted in the sifting process of the MDEEMD algorithm (Mandic et al., 2013). We then implement a nonlinear 2D data filtering scheme by utilizing the 2D filter bank resulting from the modified MDEEMD method. A simulation investigation is presented to show the improvement from the conventional MDEEMD method. To demonstrate the practical application, the proposed method is utilized in real 2D magnetic field data as an efficient 2D nonlinear filtering process. We also provide the results obtained from the MEMD and the 3D analytic signal enhancement for comparison.

2. Methods

2.1. MDEEMD method

The method of MDEEMD (Wu et al., 2009) is an extension of its original 1D EMD and EEMD algorithms (Appendix A). To design the MDEEMD algorithm, the extension from 1D to 2D is a key step. The further extension to three or more dimensional decomposition is straightforward because the identical procedure can be repeatedly executed on the succeeding dimension. After all the dimensions are decomposed, a comparable minimal scale combination principle is employed to attain the MDEEMD components. The strategy of the method is modified and described briefly as follows. The details of the original approach can be found in the contribution of Wu et al. (2009).

Mathematically, let us present a 2D spatial data set in an i by j matrix form

$$X(i,j)=\begin{pmatrix} x_{1,1} & x_{1,2} & \cdots & x_{1,j} \\ x_{2,1} & x_{2,2} & \cdots & x_{2,j} \\ \vdots & \vdots & \vdots & \vdots \\ x_{i,1} & x_{i,2} & \cdots & x_{i,j} \end{pmatrix} \tag{1}$$

At first, EEMD is performed in one direction of $X(i,j)$, horizontal direction for instance, to decompose the data of each row into m components, then to collect the components of the same level from the result of each row decomposition to constitute a 2D spatial data of that level. Therefore, m set of 2D spatial data as denoted in Eq. (2) are obtained.

$$\begin{aligned} RX(1,i,j)&=\begin{pmatrix} rx_{1,1,1} & rx_{1,1,2} & \cdots & rx_{1,1,j} \\ rx_{1,2,1} & rx_{1,2,2} & \cdots & rx_{1,2,j} \\ \vdots & \vdots & \vdots & \vdots \\ rx_{1,i,1} & rx_{1,i,2} & \cdots & rx_{1,i,j} \end{pmatrix} \\ RX(2,i,j)&=\begin{pmatrix} rx_{2,1,1} & rx_{2,1,2} & \cdots & rx_{2,1,j} \\ rx_{2,2,1} & rx_{2,2,2} & \cdots & rx_{2,2,j} \\ \vdots & \vdots & \vdots & \vdots \\ rx_{2,i,1} & rx_{2,i,2} & \cdots & rx_{2,i,j} \end{pmatrix} \\ &\vdots \\ RX(m,ij)&=\begin{pmatrix} rx_{m,1,1} & rx_{m,1,2} & \cdots & rx_{m,1,j} \\ rx_{m,2,1} & rx_{m,2,2} & \cdots & rx_{m,2,j} \\ \vdots & \vdots & \vdots & \vdots \\ rx_{m,i,1} & rx_{m,i,2} & \cdots & rx_{m,i,j} \end{pmatrix} \end{aligned} \tag{2}$$

where $RX(1,i,j)$, $RX(2,i,j)$,…, and $RX(m,i,j)$ are the m sets of 2D spatial data as stated (here we use R to indicate row decomposing). The relation between Eqs. (1) and (2) can be expressed as

$$X(i,j)=RX(1,i,j)+RX(2,i,j)+\cdots+RX(m,i,j) \tag{3}$$

More specifically speaking, the first row of the matrix *RX(m,i,j)* is the m^{th} EEMD component decomposed from the first row of the matrix *X(i,j)*. The second row of the matrix *RX(m,i,j)* is the m^{th} EEMD component decomposed from the second row of the matrix *X(i,j)*, and so on.

Suppose that the previous decomposition is along the *x* direction, the next step is to decompose each one of the previously row-decomposed components, *RX(1,i,j)*, *RX(2,i,j)*,..., and *RX(m,i,j)*, in the *y* direction into *n* components. This step will generate *n* components from each *RX* component in Eq. (2). For example, the component *RX(1,i,j)* will be decomposed into *CRX(1,1,i,j)*, *CRX(1,2,i,j)*,...,*CRX(1,n,i,j)*; *RX(2,i,j)* will be decomposed into *CRX(2,1,i,j)*, *CRX(2,2,i,j)*,..., *CRX(2,n,i,j)*; *RX(m,i,j)* will be decomposed into C*RX(m,1,i,j)*, *CRX(m,2,i,j)*,..., *CRX(m,n,i,j)* where *C* means column decomposing. The equations of these relations are

$$\begin{aligned} RX(1,i,j) &= CRX(1,1,i,j) + CRX(1,2,i,j) + \cdots + CRX(1,n,i,j) \\ RX(2,i,j) &= CRX(2,1,i,j) + CRX(2,2,i,j) + \cdots + CRX(2,n,i,j) \\ &\vdots \\ RX(m,i,j) &= CRX(m,1,i,j) + \mathrm{CRX}(m,2,i,j) + \cdots + CRX(m,n,i,j) \end{aligned} \tag{4}$$

Finally, the 2D decomposition will result in $m \times n$ matrices which are the 2D EEMD components of the original data *X(i,j)*. The matrix expression for the result of the 2D decomposition is

$$CRX(m,n,i,j) = \begin{pmatrix} crx_{1,1,i,j} & crx_{2,1,i,j} & \cdots & crx_{m,1,i,j} \\ crx_{1,2,i,j} & crx_{2,2,i,j} & \cdots & crx_{m,2,i,j} \\ \vdots & \vdots & \vdots & \vdots \\ crx_{1,n,i,j} & crx_{2,n,i,j} & \cdots & crx_{m,n,i,j} \end{pmatrix} \tag{5}$$

where each element in the matrix *CRX* is an $i \times j$ sub-matrix representing a 2D EEMD decomposed component. We use the arguments (or suffixes) *m* and *n* to represent the component number of row decomposition and column decomposition, respectively rather than the subscripts indicating the row and the column of a matrix. To simplify the notation, Eq. 5 is rewritten as

$$CRX(m,n) = \begin{pmatrix} crx_{1,1} & crx_{2,1} & \cdots & crx_{m,1} \\ crx_{1,2} & crx_{2,2} & \cdots & crx_{m,2} \\ \vdots & \vdots & \vdots & \vdots \\ crx_{1,n} & crx_{2,n} & \cdots & crx_{m,n} \end{pmatrix} \tag{6}$$

Notice that the *m* and *n* indicate the number of components resulting from row (horizontal) decomposition and then column (vertical) decomposition, respectively. In other words, the suffix *m* indicates the m^{th} EEMD component of the row decomposition, and *n* designates the n^{th} component of the column decomposition after row decomposition. That is, sub-matrix $crx_{m,n}$ is a collection of the n^{th} component resulting from the column decomposition of the previous m^{th} EEMD component of row decomposition. The decomposition can start with row or column; both ways are acceptable. However, these $m \times n$ element matrices are just detailed components representing fragmentary features of 2D objects. A strategy to integrate the detailed components to a significant 2D feature is to perform the comparable minimal scale combination principle (Wu et al., 2009). In other words, by combining the components of the same scale or the comparable scales with minimal difference will yield a 2D feature with best physical significance. This is a fairly easy task when the matrix shown in Eq. (6) is available. The components of the first row and the first column are approximately the same or comparable scale although their scales are increasing gradually along the row or column. Therefore, combining the components of the first row and the first column will obtain the first complete 2D component ($C2D_1$). The subsequent process is to perform the same combination technique to the rest of the components. For example, if $m = n = 4$, the combining procedure is expressed by three pairs of orthogonal arrows as shown in Eq. (7).

$$CRX(4,4) = \begin{array}{|c|c|c|c|} \hline crx_{1,1} & crx_{2,1} & crx_{3,1} & crx_{4,1} \\ \hline crx_{1,2} & crx_{2,2} & crx_{3,2} & crx_{4,2} \\ \hline crx_{1,3} & crx_{2,3} & crx_{3,3} & crx_{4,3} \\ \hline crx_{1,4} & crx_{2,4} & crx_{3,4} & crx_{4,4} \\ \hline \end{array} . \tag{7}$$

Consequently, the complete 2D components are

$$\begin{aligned} C2D_1 &= \sum_{m=1}^{4} crx_{m,1} + \sum_{n=1+1}^{4} crx_{1,n} = crx_{1,1} + crx_{2,1} + crx_{3,1} + crx_{4,1} \\ &\quad + crx_{1,2} + crx_{1,3} + crx_{1,4} \\ C2D_2 &= \sum_{m=2}^{4} crx_{m,2} + \sum_{n=2+1}^{4} crx_{2,n} = crx_{2,2} + crx_{3,2} + crx_{4,2} \\ &\quad + crx_{2,3} + crx_{2,4} \\ C2D_3 &= \sum_{m=3}^{4} crx_{m,3} + \sum_{n=3+1}^{4} crx_{3,n} = crx_{3,3} + crx_{4,3} + crx_{3,4}, \end{aligned}$$

and

$$C2D_4 = \sum_{m=4}^{4} crx_{m,4} + \sum_{n=4+1}^{4} crx_{4,n} = crx_{4,4} + 0 = crx_{4,4}.$$

A general equation for the combining procedure to generate complete 2D components (*C2D*) is

$$C2D_l = \sum_{m=l}^{m} crx_{m,l} + \sum_{n=l+1}^{n} crx_{l,n} \tag{8}$$

where *l* denotes the level of the *C2D*, and

$$\begin{aligned} l &= m = n \quad \text{if } m = n, \\ l &= m \quad \text{if } m<n, \\ l &= n \quad \text{if } m>n, \end{aligned} \tag{9}$$

Following the convention of 1D EMD, the last component of the complete 2D components is called residue.

The decomposition strategy can be extended without difficulty to higher or any dimensional data. For a 3D data cube of $i \times j \times k$ elements, the multidimensional EMD decomposition will yield detailed 3D components of $m \times n \times q$ where *m*, *n* and *q* are the number of the IMFs decomposed from each dimension having *i, j, and k* elements, respectively. The matrix expression for the result of the 3D decomposition is *TCRX*(*m,n,q,i,j,k*) where *T* denotes the depth (or time) decomposition. Based on the comparable minimal scale combination principle as applied in the 2D case, the number of complete 3D components will be the smallest value of *m*, *n* and *q*. The general equation for deriving 3D components is

$$C3D_l = \sum_{m=l}^{m}\sum_{n=l}^{n} tcrx_{m,n,l} + \sum_{m=l+1}^{m}\sum_{q=l+1}^{q} tcrx_{m,l,q} + \sum_{n=l+1}^{n}\sum_{q=l+1}^{q} tcrx_{l,n,q} \tag{10}$$

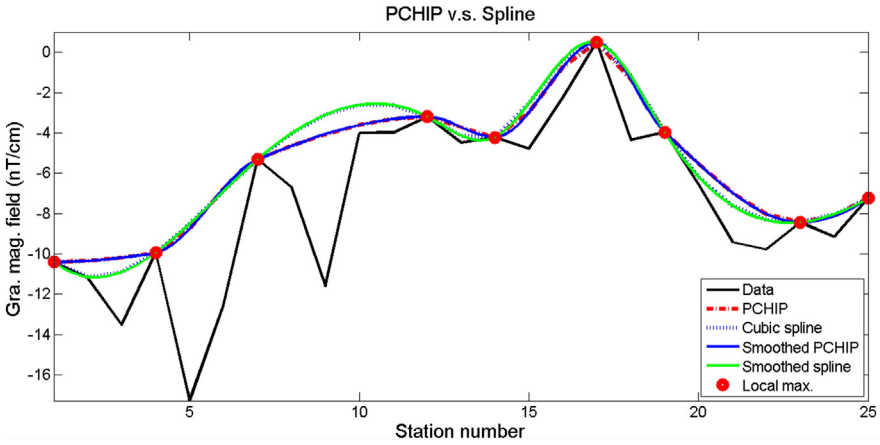

Fig. 1. Comparison of data fitted with a standard cubic polynomial spline and the PCHIP. The data set is a typical gradient magnetic survey line of the field example. The PCHIP is monotonic, and fits closer to the data.

where *tcrx* indicates the sub-matrix contained in the matrix *TCRX* (m,n,q,i,j,k). Building on the convention introduced in Eq. 5, matrix *TCRX*(m,n,q,i,j,k) is a 3D matrix having $m \times n \times q$ elements, and each element is a 3D sub-matrix having $i \times j \times k$ elements. In reality, the IMFs number of each trace is subject to the aim of the study and the data attribute. In our examples, it is an integer between 7 and 9 at most, and the higher index IMFs are close to the residue which can be neglected. To avoid unnecessary computations, we only use the first six IMFs in each direction for constructing the multi-dimensional EEMD components, and eliminate the rest components if the IMFs number is greater than six. In extreme cases where the IMFs number differs notably between traces even in the same dimension, higher amplitude noise should be added in implementing the EEMD algorithm to provide enough IMF scales for sifting the trace formerly having too few IMFs. We call the procedure "regulation". Investigators can regulate the number of IMFs to optimize the computation because there is no need to process insignificant components throughout the analysis. To perform the comparable minimal scale combination, the same number of IMFs in each dimension is also suggested.

The MDEEMD method has several advantages. For instance, the sifting procedure of the MDEEMD is a combination of one dimensional sifting. It employs 1D curve fitting in the sifting process of each dimension, and has no difficulty as encountered in the 2D EMD algorithms using surface fitting which has the problem of determining the saddle point as a local maximum or minimum. Another advantage of using the MDEEMD method is that the mode mixing is reduced significantly due to the function of the EEMD (Appendix A). The most advantageous property of the MDEEMD method is that it is ready to apply to data of any dimension. Although it can be extended to any dimensional data, we only present 2D examples for practical reasons because the computation time of higher dimensional data will be at least proportional to the number of the IMFs of the succeeding dimension. It could exceed the computation capacity of a PC based geophysical data processing system especially when the number of the ensemble members in the EEMD algorithm is large.

2.2. Interpolation method

The essential procedure of the EMD is sifting, which separates undulations of different characteristic scale by removing the incompatible fluctuations and riding waves at a given level of sifting (Appendix A). Those removed parts are left for the next level of sifting. By repeating

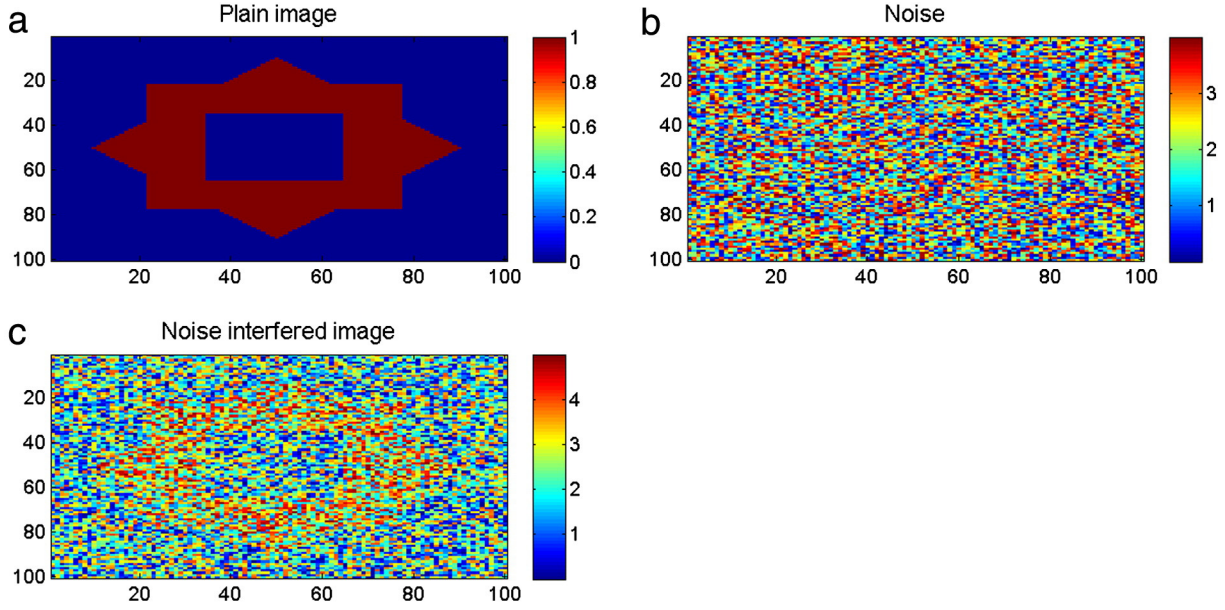

Fig. 2. Synthesis of the noise interfered image. (a) Plain image with pixel values between 0 and 1. (b) Uniformly distributed random noise with pixel values between 0 and 4. (c) Image synthesized by adding the random noise (b) on to plain image in (a).

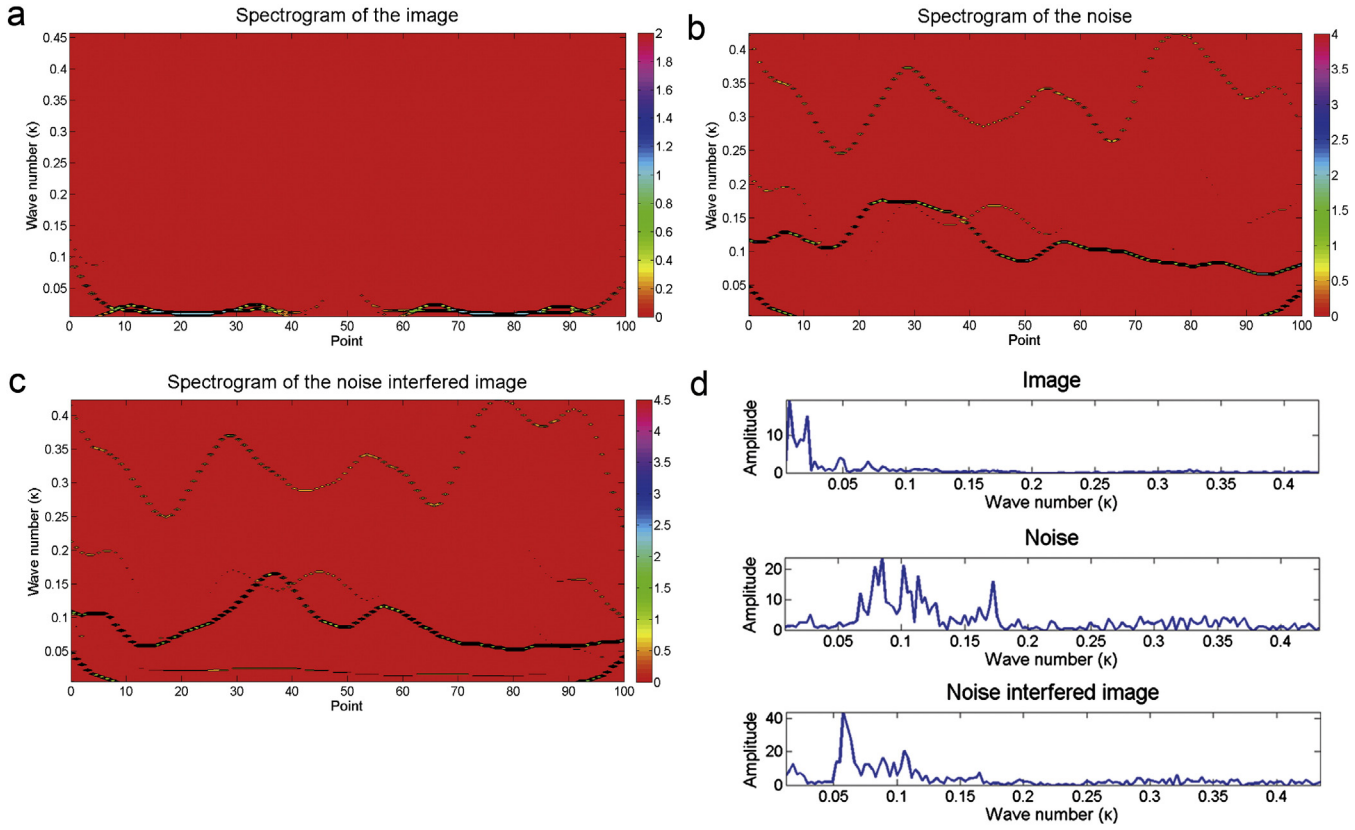

Fig. 3. Spectrogram and marginal spectra of trace 51 selected from the model image. (a) Plain image. (b) Noise. (c) Noise interfered image. (d) Marginal spectra of the image, noise, and noise interfered image. The color map is in HSV (hue, saturation and value) color space which makes the energy distribution more distinct, but the colors of the minimum and maximum data are very close.

the sifting process, a series of IMFs representing signals ranging from high frequency to low frequency are retrieved to achieve a dyadic filter bank (Flandrin et al., 2004; Wu and Huang, 2009) which is a set of filters that the frequency ranges of the neighboring filters are partly related. The first step of performing sifting is to determine the upper and lower envelopes encompassing all the data by using the spline method, in

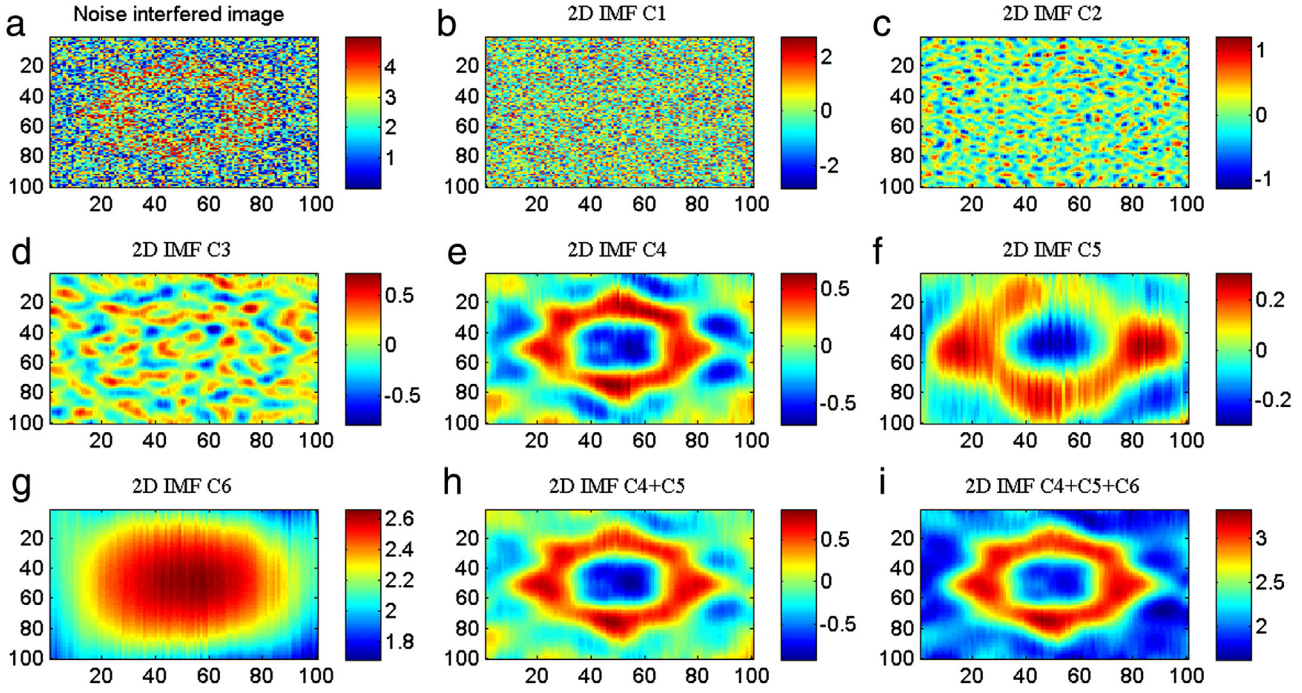

Fig. 4. Filter bank and filtering simulation of the MDEEMD with cubic spline interpolation. (a) Noise interfered image (b) to (g) displaying the 2D filter bank components from C1 to C6, respectively. Components after C6 are neglected due to lack of physical meaning. (h) Image reconstructed by using components C4 and C5. (i) Image reconstructed by using components C4, C5, and C6.

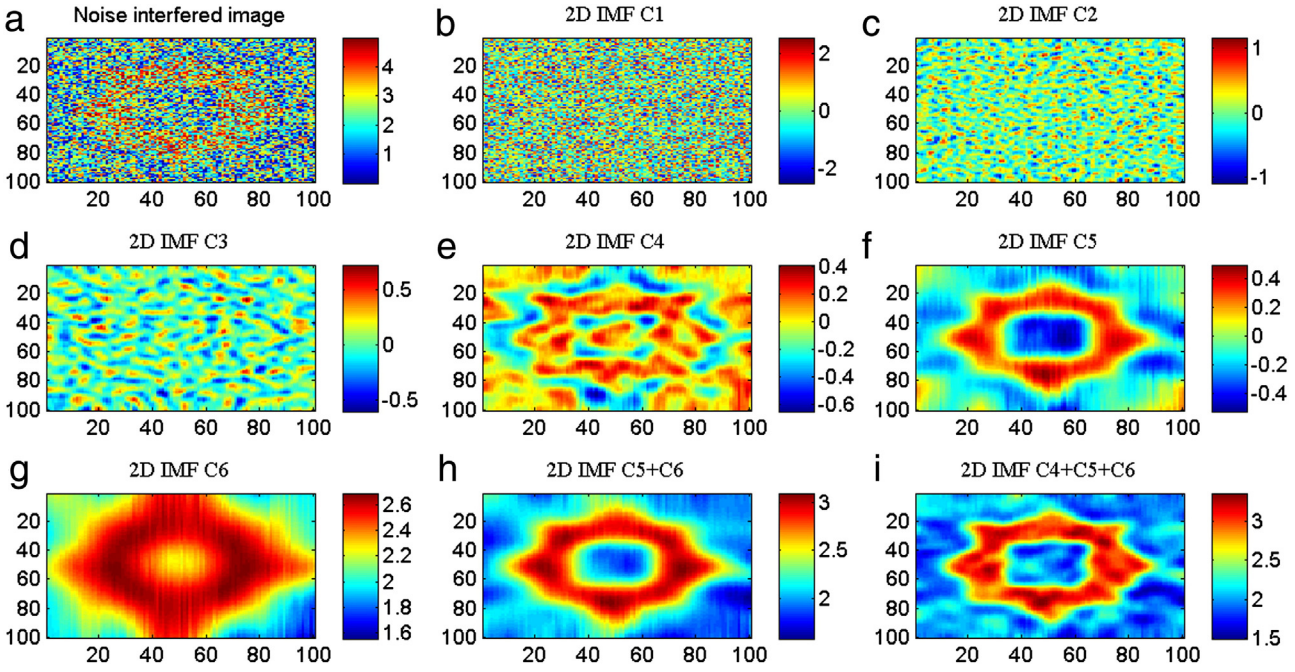

Fig. 5. Filter bank and filtering simulation of the MDEEMD with PCHIP interpolation. (a) Same noise interfered image as shown in Fig. 4a. (b) to (g) displaying the 2D filter bank components from C1 to C6, respectively. Similar to the cubic spline result, components after C6 are neglected due to lack of physical meaning. (h) Image reconstructed by using components C5 and C6. (i) Image reconstructed by using components C4, C5, and C6.

which a standard cubic polynomial spline technique is widely used to interpolate the data. The spline algorithm implements the interpolation with continuous derivatives to give a smooth result. This is adequate if the data being fitted are smooth or oscillating with high frequency, otherwise artificial local extrema will be generated due to the violation of monotonicity (no wiggling). To avoid the unrealistic smooth and redundant computations, we employ piecewise cubic Hermite interpolating polynomial (PCHIP) to fit the data. By trading off some smoothness for stability, the PCHIP fits the given data with a function that preserves the character and monotonicity of the data being interpolated (Kahaner et al., 1988). Because no higher degree (higher than 3) curves are involved and because the monotonicity constrain is satisfied in the interpolation, the PCHIP reduces the computation cost and increases the stability of curve fitting (Wolberg and Alfy, 2002). It is especially useful for sifting the lower frequency components in the EMD data sifting because it reduces more undesired artificial extrema in the lower frequency components than in the higher frequency components. This is obvious by considering the fact that at the same sample interval, the lower frequency components are better sampled than the higher frequency components. If any monotonicity is found in the lower frequency components, it should be respected rather than replaced by artificial wiggles resulting from standard cubic polynomial spline. To have a more stable interpolation particularly at the ends of the signals, we moreover adopt the slope extrapolation technique (Chen and Jeng, 2013) to alleviate the end effect problem. We determine the end points by extrapolating the slope estimated by the two preceding (the right end) or following points (the left end). In our experiences, the major discrepancy between standard cubic polynomial spline and PCHIP usually appears in the lower frequency components. Fig. 1 shows a set of real data fitted with the PCHIP and a standard non-monotone cubic interpolation (cubic spline).

Similar sifting scheme for MEMD can be found in Rehman and Mandic (2010c, 2011) where the local mean of the standard EMD is replaced by the mean of multivariate envelope curves. By using the quaternion calculation, the MEMD results in better mode alignment than the standard EMD (Rehman and Mandic, 2010a).

The idea of using Hermite polynomials or adopting optimization in the interpolation is also suggested by Mandic et al. (2013).

2.3. Data reconstruction and filtering

Once the filter bank is established, it should be ready to implement a nonlinear filter by examining the geological significance of each IMF in the filter bank, and then reconstruct the data with the selected IMFs. Theoretically, for an N point data set, the total number of IMFs decomposed is approximately $\log_2 N$ (Wu and Huang, 2009). As a multidimensional data set is considered, the complete multidimensional components (CMDCs) are achieved in accordance with the comparable minimal scale combination principle which implies that the CMDCs number is the smallest number of the IMFs obtained among all directions. Thereby, it is still a number derived from a given single dimension. It should be noted that the CMDCs are combined signals of comparable minimal scale and are not IMFs, because they do not satisfy their conditions. In practice, a common length of a geophysical data set like e.g. in one dimension is roughly between 512 and 4096; thus, the most possible IMFs number of a geophysical data set is an integer between 9 and 12, approximately. Based on our experiences and the finding of Jeng et al. (2007), the number of the CMDCs with geological significance in the examples of this study is generally less than one third of the total in the filter bank, and it is feasible to select the best combination from such a small number of IMFs in a few tries.

3. Simulation example

To assess the effect of the proposed method, we carried out a simulation of noise removal on a noise interfered image. Fig. 2a shows the plain image of a simple eight-pointed star with a square window in the middle. We added a four-fold uniformly distributed white Gaussian random noise (Fig. 2b) on to the plain image to synthesize a noise interfered image of −12 dB corresponding to a signal-to-noise ratio (SNR) of 1:4 (Fig. 2c). The SNR is commonly expressed on the logarithmic dB scale for evaluating the image resolution or the strength of a signal.

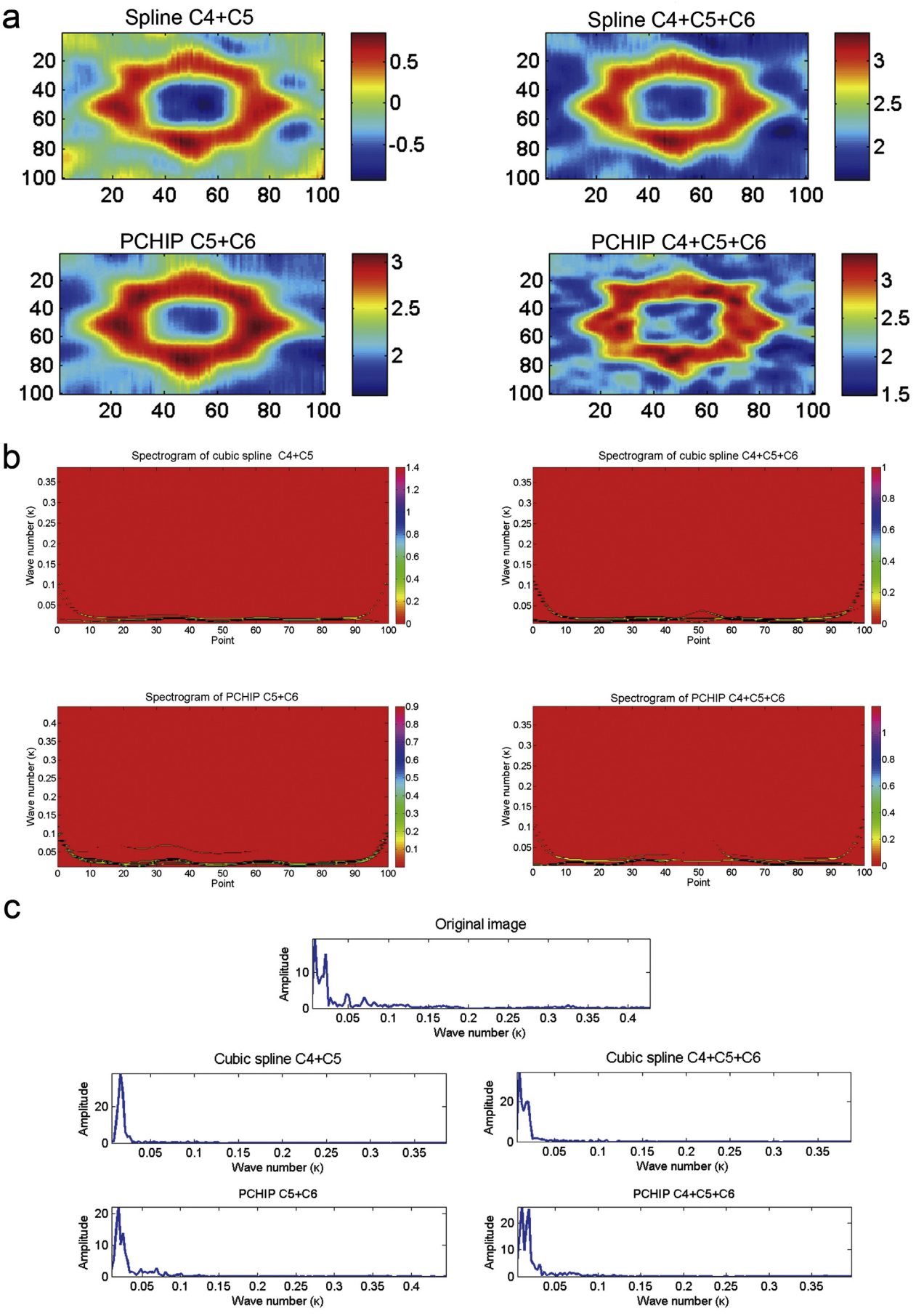
a
Spline C4+C5
Spline C4+C5+C6
PCHIP C5+C6
PCHIP C4+C5+C6
b
Spectrogram of cubic spline C4+C5
Spectrogram of cubic spline C4+C5+C6
Spectrogram of PCHIP C5+C6
Spectrogram of PCHIP C4+C5+C6
Wave number (κ)
Point
c
Original image
Cubic spline C4+C5
Cubic spline C4+C5+C6
PCHIP C5+C6
PCHIP C4+C5+C6
Amplitude
Wave number (κ)

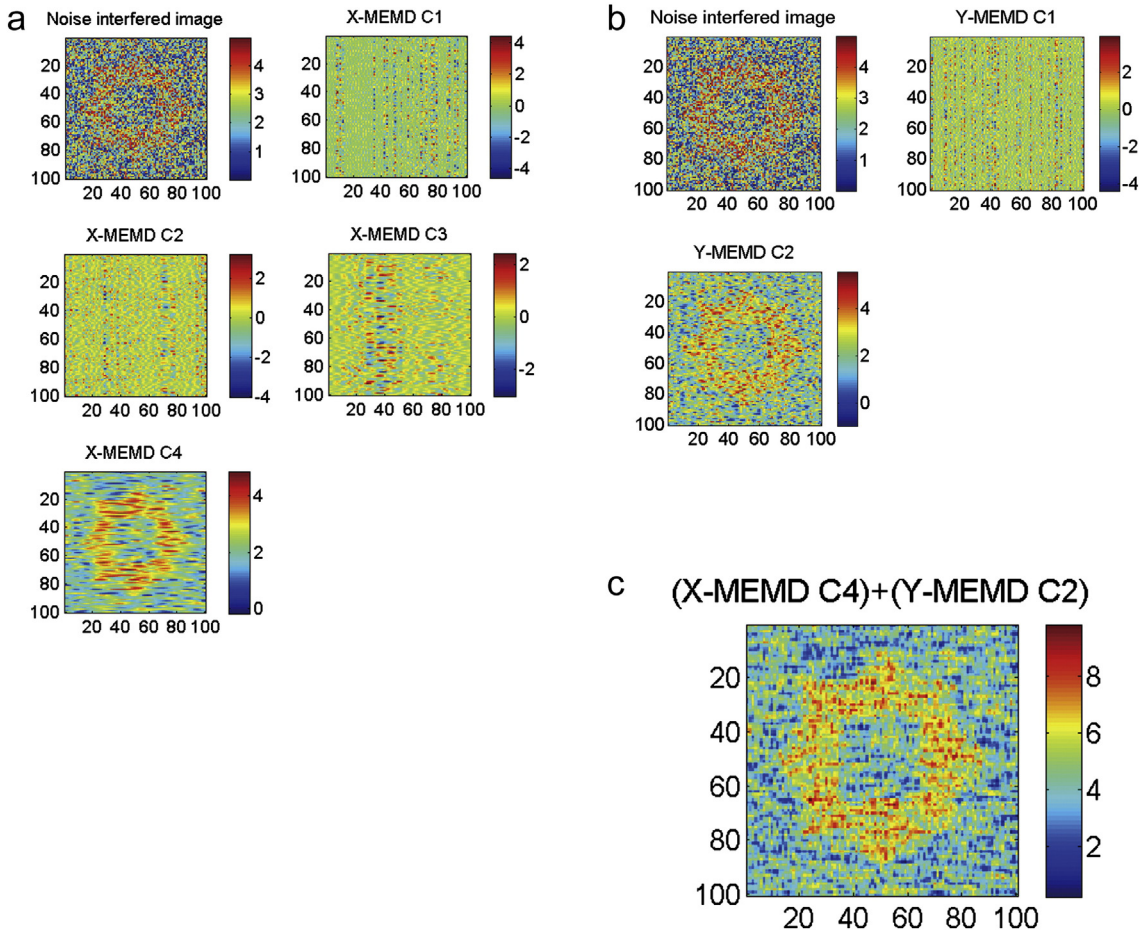

Fig. 7. Two directional filter banks and filtering simulation of the MEMD. (a) Horizontal filter bank. (b) Vertical filter bank. (c) Image reconstructed by using components of horizontal C4 and vertical C2. The resultant image is obtained by using an equal-weighted and un-normalized combination scheme.

The −12 dB SNR should be rigorous for testing a filter because typical SNR values for an image with good resolution is about +40 dB (100:1, i.e. signal amplitude is 100 fold the noise) on average (Huynh-Thu and Ghanbari, 2008). However, due to the difference between geophysical data and image pixels, the same SNR value may not have the same effect on both kinds of data. In addition to the visual demonstration, we provide spectrograms and marginal spectra (Fig. 3) obtained from a 1-D EEMD decomposition for comparing the instantaneous frequency and energy distribution of the signal, noise, and noise interfered image. It can be easily seen that no negative frequencies are involved; however, the spectrograms of signal and noise are overlapping in the very low frequency range (<0.1 wave-number).

We tested the MDEEMD on the noise interfered image with cubic spline and PCHIP interpolation algorithms separately. Fig. 4 shows the 2D filter bank (Fig. 4b to g) resulting from the MDEEMD with cubic spline interpolation. The high frequency band of the added random noise was extracted mostly in components C1 and C2. Component C3 contains the lower frequency noise with some edge information of the signal. Components C4, C5, and C6 carry the star and window signals where most of them are extracted in C4. To remove the noise, we reconstruct the image by using the components of significant features. Because the filter bank is dyadic, the signal is unable to reside in one single component and the instantaneous frequencies of the noise and of the signal part may overlap. However, the signal should not be affected by removing the noise components because the IMFs are orthogonal. As proposed by Huang et al. (1998), if the frequency band of one IMF coincides with that of the other (it is called leakage), EMD can still separate the two IMFs. Of course, in the Fourier concept, the two IMFs are not orthogonal, but it would not cause a problem in the EMD. This is one of the major differences between EMD and Fourier theory, and that is why we stress that the EMD filter bank is dyadic. In this case, obviously components 4, 5, and 6 capture parts of the signal. Fig. 5 displays the same noise interfered image (Fig. 5a) processed by using the MDEEMD with PCHIP interpolation algorithms. Fig. 5b to g are the components of the derived 2D filter bank. Compared with Fig. 4, 5 contains almost no signal information in C3. The signals of star and window are distributed in C4, C5, and C6 where C4 captures some signals with background information and lower frequency range of the noise, C5 contains most information of the signals, and C6 exhibits strong edge information of the star signal. It should be noted that in both filter banks, the signal information resides in components 4, 5, and 6 but distributes differently. Results of the two best reconstructions of both algorithms and their spectrograms and marginal spectra are displayed in Fig. 6. By comparing the signal image spectrogram (Fig. 3a) with those of the reconstructed images achieved by using the PCHIP and cubic spline algorithms (Fig. 6b), the PCHIP spectrograms are more similar to the signal image spectrogram. The marginal spectra in Fig. 6c also show that better results are obtained by using the PCHIP algorithm because the PCHIP marginal spectra gain the signal energy in the frequency range higher than 0.03 wave number and the cubic spline marginal spectra fail.

The spectrograms and marginal spectra indicate that the combination of components 4, 5 and 6 derived by using the PCHIP algorithm

Fig. 6. Visual and quantitative comparisons of the two interpolation methods. (a) Two best reconstructed images of both methods. (b) Spectrograms of trace 51 selected from images shown in (a). (c) Marginal spectra of trace 51 selected from the original image and images shown in (a).

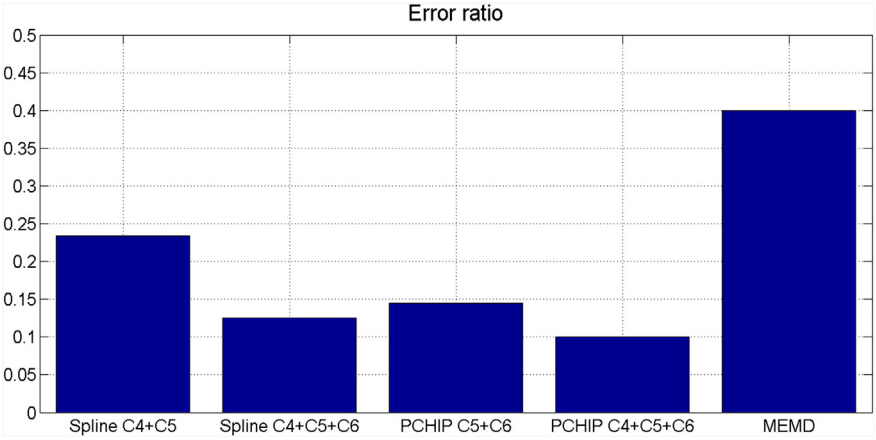

Fig. 8. Error ratios of the four best MDEEMD reconstructions and the compatible MEMD result. The error ratio (Err) is defined as Err = 1-Corr where Corr is the correlation coefficient between the filtered result and the original image.

contains more signal information than that of the cubic spline. It is also noted that during the sifting, the PCHIP interpolation reduces more undesired artificial extrema in the lower frequency components (higher index IMFs) than in the higher frequency components (lower index IMFs); therefore, the signal content is moved towards higher index IMFs containing lower frequency signals.

To make an objective comparison and give more insight of the EMD based multidimensional filtering scheme, we also present the results acquired from MEMD. Fig. 7 demonstrates the MEMD filter bank of this example. We applied the MEMD to the noise interfered image both horizontally (Fig. 7a) and vertically (Fig. 7b). We then reconstructed the image by combining the significant components selected from both filter banks (Fig. 7c). The reconstruction process is a simple equal-weighted and un-normalized addition. In this simulation example, the signal information is concentrated in one component in both filter banks, allowing the selection to be done visually.

Fig. 8. shows error ratios of all the methods employed in the simulation example. It should be noted that the result just gives a quick quantitative comparison for the specific example, and may not be adequate for other cases.

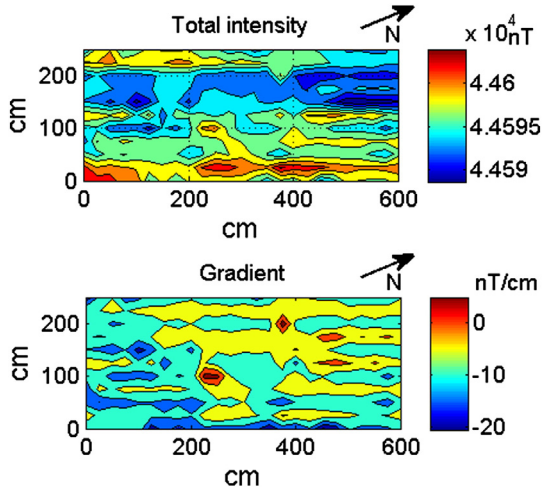

Fig. 9. Original magnetic data measured at the Chubin relic. (a) Total intensity data. (b) Vertical magnetic gradient data acquired by using a gradiometer of two sensors with 0.5 m spacing. The bottom sensor was 1 m above the ground. Data source is from Jeng et al., 2003. The "NE-SW" trend is about horizontal in the figure by referring to the marked north direction.

4. Field example

To test the effect of the proposed method in real data processing and to evaluate if it is competitive with other techniques of signal enhancement and filtering, we applied the PCHIP MDEEMD method to a set of 2D magnetic data acquired at an archaeological site by Jeng et al. (2003). The 6 m × 3 m survey grid with 0.25 m intervals was established within the Chubin relic which is situated in the mountainous range of central Taiwan. The survey target was three slate caskets excavated previously and then reburied in a thin layer of soil and broken slate fragments. The surface was covered by unwoven cloth to prevent growth of vegetations. Both total intensity and gradient data were measured by placing the bottom sensor 1 m above the ground and the top sensor 0.5 m higher than the bottom sensor. Totally 11 survey lines with 275 (25 × 11) grid points were laid out in the survey area, and the base station is located at the first grid point. The field operator reoccupied the base station every 10 to 40 minutes for time correction. Fig. 9 shows maps of the original total intensity (Fig. 9a) and gradient data (Fig. 9b). The magnetic responses of the buried caskets were interfered by strong low frequency noise bands running in an NE-SW direction. The gradient data acquisition is generally capable of removing the remote and regional effects; however, improvements are limited in this case.

In addition to the drift (trend) of the magnetometer, the total intensity data are affected by background noise like the diurnal and secular variation. A common practice of magnetic data processing is to perform time correction ahead of any further procedure. Evidently, it is conceivable that more efforts should be made in the field for collecting reliable base station data. We are expecting that the proposed method may be effective in removing the trend and background noise as well. For this reason and having an insight into the proposed method, we processed both the original total intensity data and the time corrected total intensity data to investigate the filtering effects. For the gradient data no time corrections are needed, and only the de-meaned (deviation from the mean) was performed because the gradient data are immune to the trend and background noise.

We demonstrate the2D PCHIP MDEEMD filter bank of the original total intensity data and two possible reconstructions in Fig. 10. To determine an acceptable number of the ensemble member in the MDEEMD algorithm, usually we take a small amount of data to process, start the number of the ensemble member from a small value between 5 and 10, and then gradually increase the number if the previous results are not satisfying. After an appropriate number is determined, it will be applied to process the whole data set.

Because the EEMD is a noise-assisted algorithm, the added noise increases the number of IMFs in each direction. However, we regulated the number up to six to avoid unnecessary computations. The time

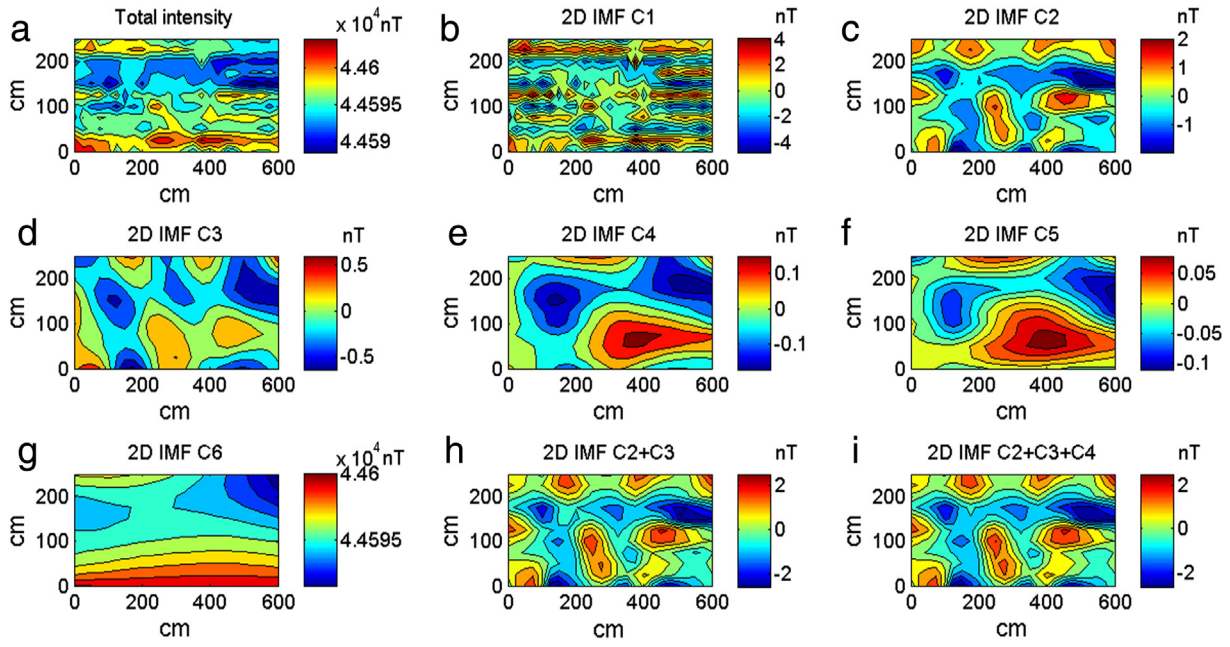

Fig. 10. MDEEMD with PCHIP interpolation filter bank and reconstructed maps of the original total intensity data. The numbers of IMFs in each direction are considerably increased due to the added noise for EEMD algorithm, but the maximum number of IMFs is regulated to six to facilitate computation. (a) Total intensity data as shown in Fig. 9a. (b) to (g) being the 2D filter bank components from C1 to C6, respectively. (h) Magnetic map reconstructed by using components C2 and C3. (i) Magnetic map reconstructed by using components C2, C3, and C4.

corrected total intensity data and de-meaned gradient data were processed by the same way, and the results are shown in Figs. 11 and 12, respectively. In the three figures, it is obvious that the C1 component extracts the horizontal (NE-SW trend on the map) noise with some high frequency background information between the trends. Components C2, C3, and C4 hold signal energy from high to low frequency. Component C5 shows some signal information, but the frequency is so low that it also contains a significant amount of the regional trend. Component C6 is close to residue which would not be considered for data reconstruction. Thus same components, i.e. C2, C3, and C4 are selected in the three filter banks for reconstructing the magnetic map showing the possible locations of the buried caskets.

To further assess the filtering extent of the proposed method, the de-meaned gradient data are also processed by using the MEMD method. The filter banks of two directions and the reconstructed maps are shown in Fig. 13. In Fig. 14, we compare the results obtained from

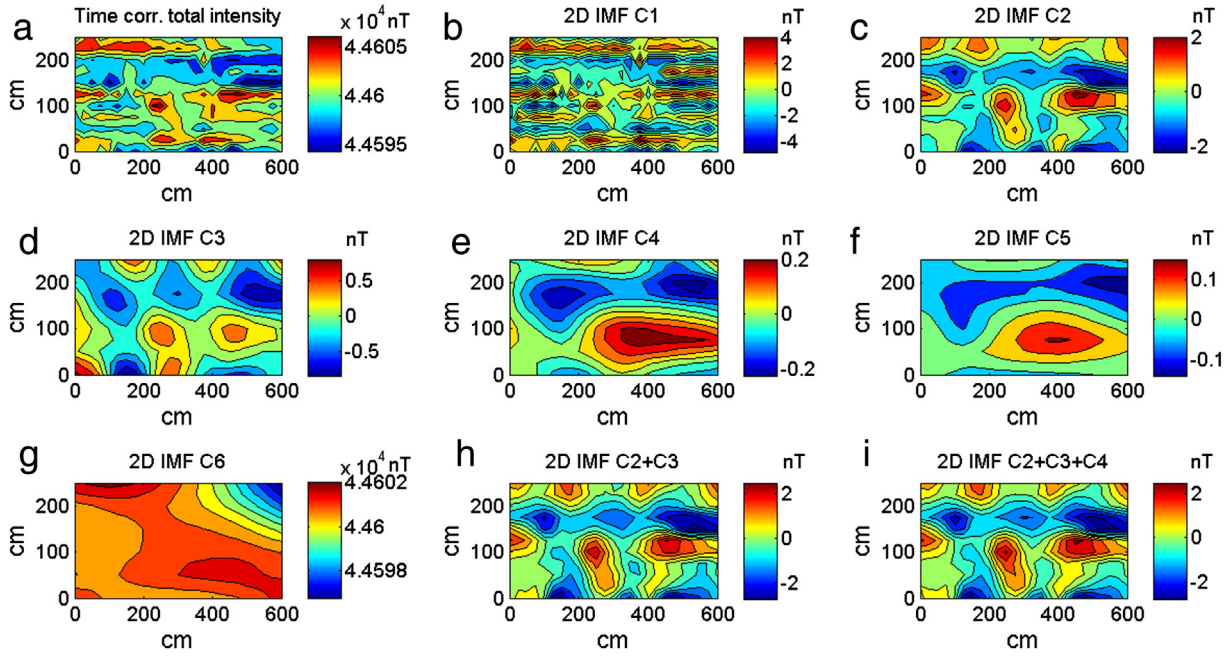

Fig. 11. MDEEMD with PCHIP interpolation filter bank and reconstructed maps of the time corrected total intensity data. (a) Time corrected total intensity (data source from Jeng et al., 2003). (b) to (g) being the 2D filter bank components from C1 to C6, respectively. (h) Magnetic map reconstructed by using components C2 and C3. (i) Magnetic map reconstructed by using components C2, C3, and C4.

MDEEMD and MEMD with the filtered result achieved by Jeng et al. (2003). Fig. 14a shows the MDEEMD reconstructed map of de-meaned gradient data. Obviously, the magnetic responses of the three caskets are significantly enhanced. The buried casket A reveals a dipole anomaly, probably indicating that the magnetization is nearly horizontal. Anomaly of casket B is slightly asymmetric, and the magnetization could down-dip to the southeast. With a strong positive anomaly, the vertical magnetization of casket C is highly possible. Fig. 14b demonstrates the MEMD reconstructed map. The pattern of magnetic anomalies is similar to that of the MDEEMD result, but the signal is weaker. Fig. 14c shows the result achieved by using the 3-D analytic signal enhancement (redrawn from Jeng et al., 2003). The 3D analytic signal enhancement is a technique for magnetic signal improvement (Hsu et al., 1996; Roest et al., 1992; Tabbagh et al., 1997) which is effective in resolving the outlines and detailed features of the source bodies. It may be premature to judge which method is the best, but with the comprehensive visual comparison we conclude that the MDEEMD filtering indeed presents a convincing result in this case.

5. Discussion and conclusions

In this study, we propose a nonlinear 2D filtering scheme by reconstructing the 2D EEMD analyzed data. Constituents of the data having different frequency characteristics can be examined in a single feature distribution. With appropriate fusions of the IMFs, it can separate the signal from the noise content of data. In the demonstrated examples, we successfully remove large parts of the noise added in the simulation data and effectively recover signal responses of buried targets by applying the proposed filtering scheme. Specially, this technique can be extended to be applicable for multidimensional data filtering, but then the main concern is to overcome the computation cost. With regard to this issue, we suggest that the number of the ensemble members in the EEMD algorithm should be chosen as small as possible. In this study, we use 40 runs for the synthetic example and 100 runs for the data example. We also found that the number of data points of each dimension may differ in real data. This could cause some difficulties in designing the computer program because the last IMF (or residue) of an uneven data set is not multidimensional. A common practice to solve this problem without sacrificing the integrity of the theory is to regulate the number of IMFs as we mentioned in Section 2.1 and demonstrate in the field example.

Although the PCHIP interpolation technique we used in the sifting is useful in our examples, we do not intend to abandon the popular smooth spline interpolation method. The PCHIP is appropriate for treating data with substantial monotonicity or of low sampling density; the smooth spline interpolation works as well otherwise.

One possible dilemma raised from the comparable minimal scale combination algorithm is that the CMDCs are not IMFs and that there could be negative frequencies existing in the combined signal. However, it should not be an issue in our case based on the following three reasons. Firstly, a geological significant event could be a combination of several IMFs (usually two or three in our case); therefore, the significant events (signals) that we tried to recover in the spatial-amplitude domain are not necessary mono-component and mono-frequency. In other words, mono-component instantaneous attributes presentation may not be the best strategy for showing geological events (Chen and Jeng, 2013). Secondly, negative frequencies are the consequence of mathematical operation, e.g. the Fourier transform or Hilbert transform. One technique in geophysical data processing is to present the data in instantaneous attributes domain by using the Hilbert transform for indentifying complex structures, and instantaneous frequency is one of the attributes. In this study, we do not deal with the instantaneous attributes, and certainly do not apply any transform. Lastly, all the IMFs are zero mean, and thus have no negative instantaneous frequencies if we perform the transform (Chen and Jeng, 2013; Huang et al., 2009). Although negative instantaneous frequencies may still occur in the attribute domain for some other reasons (Huang et al., 2009), the chance is very slim because our algorithm is not Fourier-based. If the negative instantaneous frequency is still an issue, it can be corrected by using the local averaging with the end effect removal technique (Chen and Jeng, 2013).

Although we do not deal with the MDEEMD instantaneous attributes in this study, it is still an interesting research topic deserving further investigation.

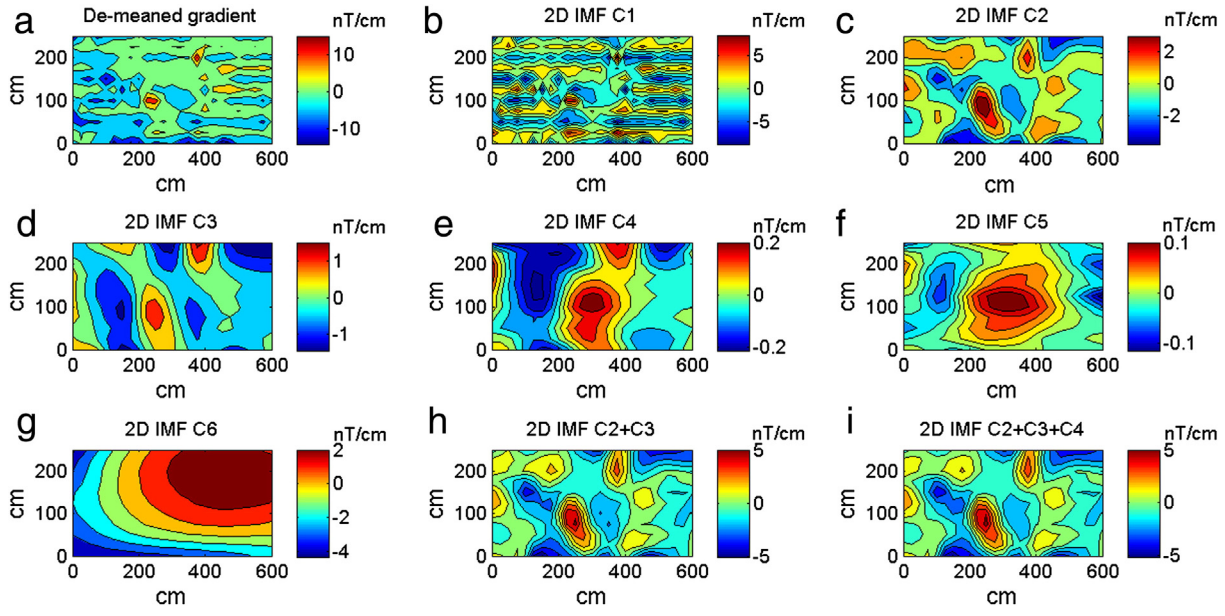

Fig. 12. MDEEMD with PCHIP interpolation filter bank and reconstructed maps of the de-meaned gradient data. (a) Original magnetic map of de-meaned gradient data (data source from Jeng et al., 2003). (b) to (g) being the 2D filter bank components from C1 to C6, respectively. (h) Magnetic map reconstructed by using components C2 and C3. (i) Magnetic map reconstructed by using components C2, C3, and C4.

Acknowledgments

We are greatly thankful for the insightful comments made by two anonymous reviewers. This research was financially supported by the National Science Council of Taiwan, ROC, Grant No. NSC 102-2116-M-003 -006 and the Ministry of Science and Technology of Taiwan, ROC, Grant No. MOST 103-2116-M-003 -008.

Appendix A. One dimensional EMD and EEMD methods

The EMD method assumes that signals arise from local oscillations, and any signal can be decomposed into a set of mono-components called intrinsic mode functions (IMFs) and a residue. The IMFs must satisfy two conditions: (1) the number of extrema (maxima and minima) and the number of zero crossings should be equal, or differ at most by one; (2) the envelope defined by the local maxima and that by the local minima are symmetrical to zero (Huang and Wu, 2008; Huang et al., 1998). In contrast to the Fourier analysis, which decomposes a signal into a sum of mono-frequency, constant-amplitude harmonics, the IMFs are amplitude/frequency-modulated oscillations that give the embedded non-stationary and nonlinear characteristics of the signal. To decompose the signal into IMFs, an adaptive, data-driven nonlinear working technique called "sifting" is carried out to reduce unwanted fluctuations and riding waves. This technique can be summarized as follows:

(a) Determine the upper and lower envelopes encompassing all the data $y(t)$ by using the spline method which interpolates between all the maxima and minima to obtain the upper and lower envelopes, respectively.
(b) Calculate the mean $m_1(t)$ of the two envelopes.

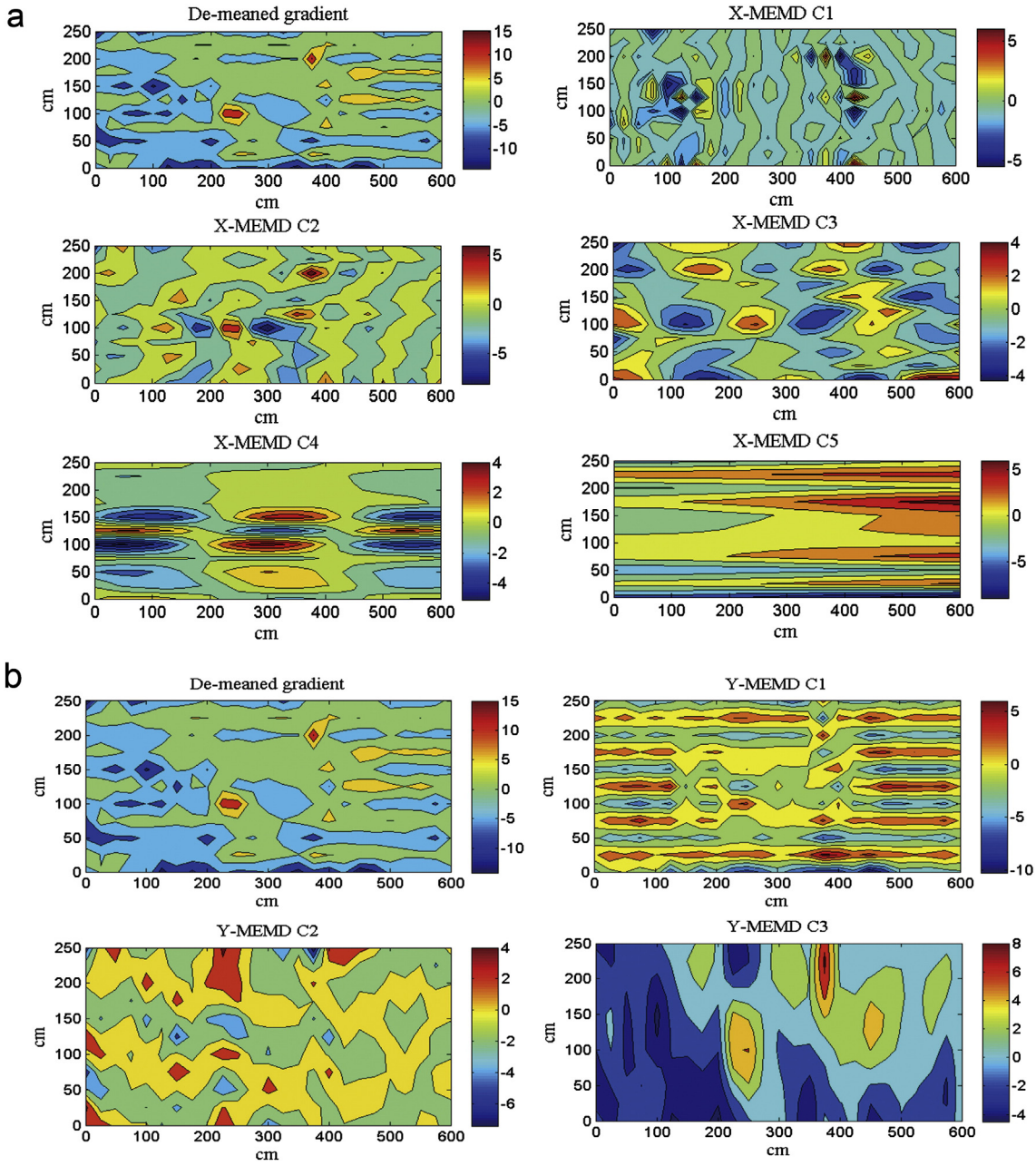

Fig. 13. MEMD filter banks and reconstructed maps of the de-meaned gradient data. (a) Horizontal (X-MEMD) filter bank. The top right map is the de-meaned gradient data. (b) Vertical (Y-MEMD) filter bank. (c) Single directional MEMD reconstructed maps: X-MEMD C2 + C3 (left); Y-MEMD C2 + C3 (right). (d) Two directional reconstruction by combining the two maps shown in (c).

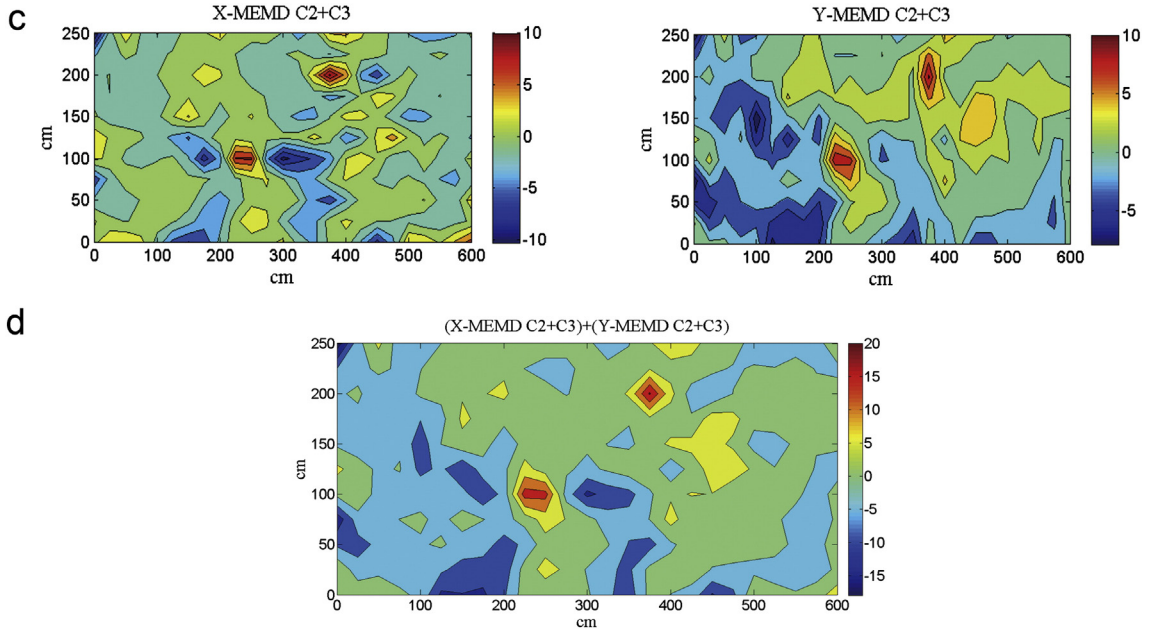

Fig. 13 (*continued*).

(c) Subtract the mean $m_1(t)$ from the data $y(t)$ to obtain the first component $h_1(t)$which is the prototype of the IMF component c_1.
(d) Test whether $h_1(t)$ is an IMF or not. If it is not, $h_1(t)$ is treated as the data, and then steps (a) to (c) will be repeated j times until the obtained $h_{1j}(t)$ satisfies the conditions of an IMF.

A criterion for the sifting process to stop is by carrying out the Cauchy type of convergence test which guarantees enough physical sense retained in the IMF components. The convergence test is performed by calculating the size of the standard deviation, SD, computed from the two consecutive sifting results. For a given data set with $S+1$ samples, the size of the standard deviation after j times of sifting, SD_j, is

$$SD_j = \frac{\sum_{t=0}^{S} \left| d_{j-1}(t) - d_j(t) \right|^2}{\sum_{t=0}^{S} d_{j-1}^2(t)} \qquad (A-1)$$

where d_j is the difference between the input data and the mean of the two envelopes at j times of sifting. Suggested values of SD_j are between 0.2 and 0.3 (Huang et al., 1998); however, this is an empirical criterion, and a rigorous justification is needed.

When $h_{1j}(t)$ satisfies the conditions of an IMF, it is designated as the IMF c_1 indicating that the first IMF decomposed from the data. Component c_1 then can be separated from the rest of the data by subtracting it from the original data, and a residue r_1 results. The residue may contain lower frequency components and is treated as the new data for generating the next level's IMF. The decomposition process is stopped when the residue r_n is less than a predetermined stoppage value or the residue becomes a monotonic function in which no more IMF can be extracted. Consequently, the original data set is iteratively decomposed into a set of IMFs and a residue as follows

$$y(t) = \sum_{i=1}^{n} c_i + r_n \qquad (A-2)$$

where c_i, $i = 1,\ldots,n$, are the n IMF components of different frequency band, and r_n is the residue after repeating the sifting procedure n times.

A frequently encountered difficulty of the EMD is mode mixing (i.e. signals of different scales are mixed in a single IMF or a signal of the same scale residing in different IMF components). Mode mixing is particularly serious when the data are attenuated or contain intermitting signal, and it can distort the physical meaning and uniqueness of an IMF. Wu and Huang (2009) proposed a new noise-assisted data analysis method—the ensemble EMD (EEMD)—to overcome the mode mixing problem. The EEMD derives each IMF component from the mean of an ensemble of the same level of IMFs, and each IMF in the ensemble consists of the signal plus a white noise of finite amplitude. The EEMD algorithm contains steps as follows:

(a) Add a white Gaussian noise series $w(t)$ of SD 1, finite amplitude, and zero mean to the original data $y(t)$, then the noise added data $Y(t)$ is

$$Y(t) = y(t) + w(t) \times R \qquad (A-3)$$

where R is the ratio of the standard deviation of the added noise amplitude to that of the data $y(t)$.
(b) Decompose the white noise added data into IMFs.
(c) Repeat step (a) and step (b) k times with different white noise series of same amplitude level each time.
(d) Obtain the (ensemble) means of corresponding IMFs of the decompositions

$$\bar{c}_j(t) = \frac{E_j(t)}{k} = \frac{1}{k}\sum_{l=1}^{k} c_{jl} \qquad (A-4)$$

where $E_j(t) = \sum_{l=1}^{k} c_{jl}$ represents the ensemble of the j^{th} level of IMF.

Because different white noise series have no correlation with one another, they cancel each other out when taking the ensemble mean, and only the signal resides if k (the number of the ensemble members) is infinitive. The added white noise series, therefore, provide uniformly reference scales in the time-frequency domain for the signal but cause

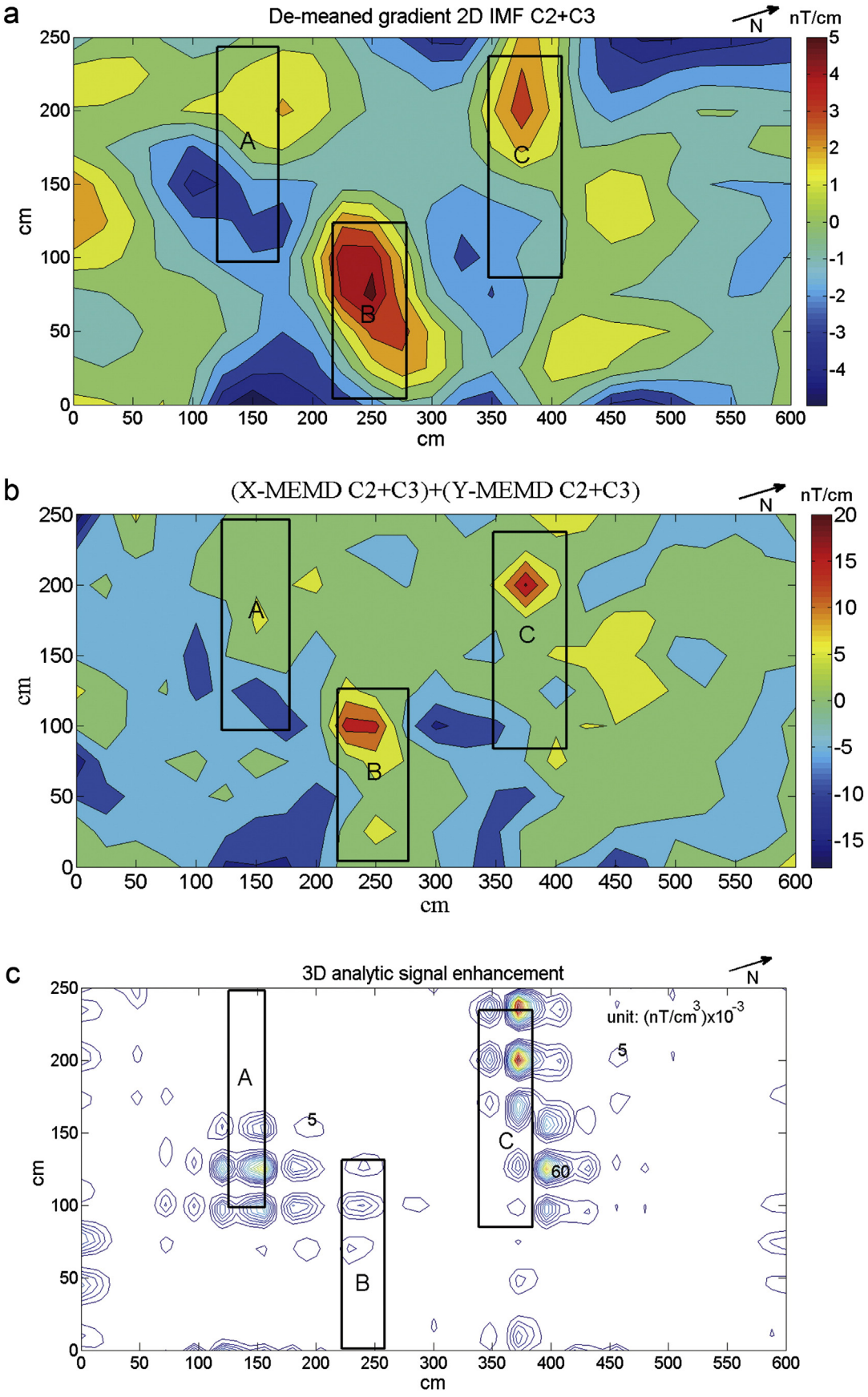

Fig. 14. Visual comparison of the representative MDEEMD result with that of other competitive methods. Rectangles A, B, and C indicate buried caskets. (a) MDEEMD reconstructed map. (b) MEMD reconstructed map. (C) 3-D analytic signal enhancement map. This sub-figure is redrawn from Jeng et al. 2003.

no interference. This approach effectively reduces the mode mixing, and is a substantial improvement over the EMD method.

References

Battista, B.M., Knapp, C., Mcgee, T., Goebel, V., 2007. Application of the empirical mode decomposition and Hilbert-Huang transform to seismic reflection data. Geophysics 72, H29–H37.

Bhuiyan, S.M.A., Attoh-Okine, N.O., Barner, K.E., Ayenu, A.Y., Adhami, R.R., 2009. Bidimensional empirical mode decomposition using various interpolation techniques. Adv. Adapt. Data Anal. 1, 309–338.

Chen, C.-S., Jeng, Y., 2011. Nonlinear data processing method for the signal enhancement of GPR data. J. Appl. Geophys. 75, 113–123.

Chen, C.-S., Jeng, Y., 2013. Natural logarithm transformed EEMD instantaneous attributes of reflection data. J. Appl. Geophys. 95, 53–65.

Damerval, C., Meignen, S., Perrier, V., 2005. A fast algorithm for bidimensional EMD. IEEE Signal Process. Lett. 12, 701–704.

Flandrin, P., Rilling, G., Gonçalvés, P., 2004. Empirical mode decomposition as a filter bank. IEEE Signal Process. Lett. 11, 112–114.

Foufoula-Georgiou, E., Kumar, P., 1994. Wavelets in geophysics. Academic Press, (43 pp.).

Han, J., van der Baan, M., 2013. Empirical mode decomposition for seismic time-frequency analysis. Geophysics 78, O9–O19.

Hsu, S.-K., Sibuet, J.-C., Shyu, C.-T., 1996. High-resolution detection of geologic boundaries from potential-field anomalies: an enhanced analytic signal technique. Geophysics 61, 373–386.

Huang, N.E., 2001. Computer implemented empirical mode decomposition apparatus, method and article of manufacture for two-dimensional signals. US Patent 6,311,130 B1, Granted Oct. 30, 2001.

Huang, N.E., Wu, Z., 2008. A review on Hilbert-Huang transform: method and its applications to geophysical studies. Rev. Geophys. 46, 1–23.

Huang, N.E., Shen, Z.S., Long, R.M., Wu, C., Shih, H.-H., Zheng, Q., Yen, N.-C., Tung, C.-C., Liu, H.-H., 1998. The empirical mode decomposition and the Hilbert spectrum for nonlinear and nonstationary time series analysis. Proc. R. Soc. Lond. A 454, 903–995.

Huang, N.E., Wu, Z., Long, S.R., Arnold, K.C., Chen, X., Blank, K., 2009. On instantaneous frequency. Adv. Adapt. Data Anal. 1, 177–229.

Huynh-Thu, Q., Ghanbari, M., 2008. Scope of validity of PSNR in image/video quality assessment. Electron. Lett. 44, 800–801.

Jeng, Y., Chen, C.-S., 2011. A nonlinear method of removing harmonic noise in geophysical data. Nonlinear Process. Geophys. 18, 367–379.

Jeng, Y., Chen, C.-S., 2012. Subsurface GPR imaging of a potential collapse area in urban environments. Eng. Geol. 147–148, 57–67.

Jeng, Y., Lee, Y.-L., Chen, C.-Y., Lin, M.-J., 2003. Integrated signal enhancements in magnetic investigation in archaeology. J. Appl. Geophys. 53, 31–48.

Jeng, Y., Lin, M.-J., Chen, C.-S., Wang, Y.-H., 2007. Noise reduction and data recovery for a very low frequency electromagnetic survey using the nonlinear decomposition method. Geophysics 72, F223–F235.

Jeng, Y., Lin, C.-H., Li, Y.-W., Chen, C.-S., Yu, H.-M., 2011. Application of sub-image multiresolution analysis of ground-penetrating radar data in a study of shallow structures. J. Appl. Geophys. 73, 251–260.

Kahaner, D., Moler, C., Nash, S., 1988. Numerical methods and software. Prentice Hall, (384 pp.).

Lin, M.-J., Jeng, Y., 2010. Application of the VLF-EM method with EEMD to the study of a mud volcano in southern Taiwan. Geomorphology 119, 97–110. http://dx.doi.org/10.1016/j.geomorph.2010.02.021.

Linderhed, A., 2005. Variable sampling of the empirical mode decomposition of two dimensional signals. Int. J. Wavelets Multi-resolut. Inf. Proc. 3, 435–452.

Looney, D., Mandic, D.P., 2009. Multi-Scale image fusion using complex extensions of EMD. IEEE Trans. Signal Process. 57, 1626–1630.

Macelloni, L., Battista, B.M., Knapp, C.C., 2011. Optimal filtering high-resolution seismic reflection data using a weighted-mode empirical mode decomposition operator. J. Appl. Geophys. 75, 603–614.

Mandic, D.P., Rehman, N., Wu, Z., Huang, N.E., 2013. Empirical mode decomposition based time-frequency analysis of multivariate signals: the power of adaptive data analysis. IEEE Signal Process. Mag. 30 (6), 74–86.

Neukirch, M., Garcia, X., 2014. Nonstationary magnetotelluric data processing with instantaneous parameter. J. Geophys. Res. Solid Earth 119 (3), 1634–1654.

Nunes, J.C., Bouaoune, Y., Delechelle, E., Niang, O., Bunel, P., 2003. Image analysis by bidimensional empirical mode decomposition. J. Image Vision Comput. 21, 1019–1026.

Nunes, J.C., Guyot, S., Delechelle, E., 2005. Texture analysis based on local analysis of the bidimensional empirical mode decomposition. Mach. Vis. Appl. 16, 177–188.

Rehman, N., Mandic, D.P., 2010a. Empirical mode decomposition for trivariate signals. IEEE Trans. Signal Process. 58, 1059–1068.

Rehman, N., Mandic, D.P., 2010b. Quadrivariate empirical mode decomposition. Int. Symp. Neural Netw. 1–7.

Rehman, N., Mandic, D.P., 2010c. Multivariate empirical mode decomposition. Proc. R. Soc. Lond. A 466, 1291–1302.

Rehman, N., Mandic, D.P., 2011. Filter bank property of multivariate empirical mode decomposition. IEEE Trans. Signal Process. 59, 2421–2426.

Rehman, N., Park, C., Huang, N.E., Mandic, D.P., 2013. EMD via MEMD: multivariate noise-aided computation of standard EMD. Adv. Adapt Data Anal. 5 (02), 1–25 (1350007).

Rilling, G., Flandrin, P., Goncalves, P., Lilly, J.M., 2007. Bivariate empirical mode decomposition. IEEE Signal Process. Lett. 14, 936–939.

Roest, W.R., Verhoef, J., Pilkington, M., 1992. Magnetic interpretation using the 3-D analytic signal. Geophysics 57, 116–125.

Stollnitz, E.J., DeRose, T.D., Salesin, D.H., 1995. Wavelets for computer graphics: a primer, part 1. IEEE Comput. Graph. Appl. 15 (3), 76–84.

Tabbagh, A., Desvignes, G., Dabas, M., 1997. Processing of Z gradiometer magnetic data using linear transforms and analytical signal. Archaeol. Prospect. 4, 1–13.

Tanaka, T., Mandic, D.P., 2007. Complex empirical mode decomposition. IEEE Signal Process. Lett. 14, 101–104.

Wolberg, G., Alfy, I., 2002. An energy-minimization framework for monotonic cubic spline interpolation. J. Comput. Appl. Math. 143 (145–188), 188–195.

Wu, Z., Huang, N.E., 2009. Ensemble empirical mode decomposition: a noise-assisted data analysis method. Adv. Adapt. Data Anal. 1, 1–41.

Wu, Z., Huang, N.E., Chen, X., 2009. The multidimensional ensemble empirical mode decomposition method. Adv. Adapt. Data Anal. 1, 339–372.

Xu, Y., Liu, B., Liu, J., Riemenschneider, S., 2006. Two-dimensional empirical mode decomposition by finite elements. Proc. R. Soc. Lond. A 462, 3081–3096.

Xue, Y.-J., Cao, J.-X., Tian, R.-F., 2013. A comparative study on hydrocarbon detection using three EMD-based time–frequency analysis methods. J. Appl. Geophys. 89, 108–115.

Zhou, Y., Chen, W., Gao, J., He, Y., 2012. Application of Hilbert–Huang transform based instantaneous frequency to seismic reflection data. J. Appl. Geophys. 82, 68–74.